

Microwave-Assisted Synthesis of TiO₂-ZnO Oxide Systems with Enhanced Photocatalytic and Photovoltaic Activity [†]

Adam Kubiak ^{1,*}, Zuzanna Bielan ², Aleksandra Bartkowiak ³, Maciej Zalas ³,
Anna Zielińska-Jurek ², Katarzyna Siwińska-Ciesielczyk ¹ and Teofil Jesionowski ^{1,*}

¹ Faculty of Chemical Technology, Institute of Chemical Technology and Engineering, Poznan University of Technology, Berdychowo 4, PL-60965 Poznan, Poland; katarzyna.siwinska-ciesielczyk@put.poznan.pl

² Department of Process Engineering and Chemical Technology, Faculty of Chemistry, Gdansk University of Technology, Narutowicza 11/12, PL-80233 Gdansk, Poland; zuzbiela@student.pg.edu.pl (Z.B.); annjurek@pg.edu.pl (A.Z.-J.)

³ Poznan, Faculty of Chemistry, Adam Mickiewicz University, Uniwersytetu Poznanskiego 8, PL-61614 Poznan, Poland; aleksandra.bartkowiak@amu.edu.pl (A.B.); maciej.zalas@amu.edu.pl (M.Z.)

* Correspondence: adam.l.kubiak@doctorate.put.poznan.pl (A.K.); teofil.jesionowski@put.poznan.pl (T.J.); Tel.: +48-61-665-3747 (A.K.); +48-61-665-3720 (T.J.)

[†] Presented at the 2nd International Online-Conference on Nanomaterials, 15–30 November 2020; Available online: <https://iocn2020.sciforum.net/>.

Published: 15 November 2020

Abstract: A microwave method was used for the synthesis of TiO₂-ZnO oxide systems. A detailed investigation was made to study the effect of the molar ratio of components (TiO₂:ZnO=9:1, 7:3, 5:5, 3:7, 1:9) on the crystalline structure and morphology. Based on the TEM pictures, the presence of octahedral and rod-shaped titania particles and sheet zinc oxide particles had been shown. Moreover, the synthesized materials were analyzed by X-ray diffraction (XRD) and high resolution transmission electron microscopy (HR-TEM), and two crystalline forms – anatase and wurtzite were detected. The adsorption-desorption N₂ isotherms confirmed mesoporous characters of the fabricated binary oxide materials. The main goal of the work was to determine the photocatalytic activity of the obtained TiO₂-ZnO oxide systems in the degradation of phenol. Photo-oxidation tests proved that the binary oxide materials (especially the (9)TiO₂-(1)ZnO and (7)TiO₂-(3)ZnO samples) demonstrate high photocatalytic activity in the decomposition of phenol (95% after 80 min irradiation) compared with the reference titania sample. Furthermore, it was also pointed out that the dye-sensitized solar cells (DSSC's) can be a second application for the synthesized TiO₂-ZnO materials. The best photovoltaic parameters have been found in the case of the (9)TiO₂-(1)ZnO material, which was characterized by an efficiency of 8.84%. The improvement effect is caused by introducing into the TiO₂-ZnO oxide system a ZnO material with a higher conductivity band, which additionally improve the transport of electrons inside the semiconductor layer.

Keywords: titania; zinc oxide; microwave method; photocatalysis; DSSC

1. Introduction

Nowadays, the world faces enormous challenges ahead as drinkable water run short due to natural disasters associated with global warming [1,2]. The urbanization, as well as the development of the world economy, causes temperature increases in the natural environment and hence the problem with access to water [3,4]. Therefore, the possible reuse of wastewater for agricultural and industrial activities may be the best solution for the future of sustainable water management. Since these wastewaters constitute one of the most extensive possible water resources, their reuse could

offset more clean water resources [5–7]. Based on scientific knowledge, one of the leading technology for the purification of sewage is photocatalysis. Photo-oxidation process has attracted increasing attention during the past decades due to its effectiveness in rapidly degrading and mineralizing recalcitrant organic compounds such as pharmaceuticals, dyes or derivatives of phenol.

Additionally, a significant problem related to economic progress is the energy production from fossil fuels, which causes deterioration of air quality. According to the reports of the Global Health Observatory (GHO) every year, approximately 4 million people die due to air pollution. Therefore, the improvement of air quality is critical. This can be achieved by the application of dye-sensitized solar cells in energy productions, among others [8,9]. Since both of the above mentioned technologies: photocatalytic degradation of organic pollutants, as well as energy production using DSSC's are based on photo-induced processes, an important aspect is the selection of the material which will be characterized with well-defined photocatalytic as well as photovoltaic properties [10,11].

Furthermore, based on the available literature [12], it was found that the properties such as crystalline structure and morphology have a crucial role in the potential application of final materials. Among synthesis methods which allow to control the crystallinity and morphology special attention should be paid to hydrothermal treatment [13], electrospinning [14], sonochemical [15] or soft/hard template [16] methods. Nowadays, scientists are also focusing on the microwave synthesis [17,18]. This technique has many advantages such as rapid and uniform heating, energy-saving process, higher yield and shorter time of preparation, lower processing cost as well as obtaining products with narrow particle size distributions etc. [19]. Additionally, Roberts and Strauss [20] reported that microwave synthesis could be an element of a broad strategy towards environmental protections.

Taking into account the previous scientific works of our research team, as well as the lack of literature reports on the use of microwave treatment in the synthesis of mixed oxide systems, the main aim of the research was to applied the microwave synthesis for fabrication of titanium dioxide-zinc oxide materials. The obtained systems exhibited highly crystalline phases: anatase and wurtzite. Additionally, based on the TEM images, it was indicated that ZnO nanosheets were covered with nanocrystalline TiO₂ particles. The key element of the work was the potential application of the synthesised oxide systems. In the first, was specified the photocatalytic activity of the fabricated TiO₂-ZnO oxide systems in the degradation of phenol. The performed photo-oxidation tests proved that the binary oxide materials (especially the (9)TiO₂-(1)ZnO and (7)TiO₂-(3)ZnO samples) demonstrate high photocatalytic activity in the decomposition of phenol compared with the reference titania sample. Type II heterojunction has been proposed as the primary mechanism for improving the efficiency of photodegradation. Moreover, the synthesized materials have also exhibited good properties when were used as a semiconducting layers in DSSCs. The best photovoltaic parameters have been found in the case of the (9)TiO₂-(1)ZnO oxide system, which was characterized by an efficiency of 8.84%.

2. Materials and Method

2.1. Materials

TiCl₄ (97%), Zn(COO)₂·2H₂O (99.5%), polyvinylpyrrolidone (PVP, 99%) and sodium hydroxide (99.5%) were purchased from Sigma-Aldrich (USA). All reagents were of analytical grade and used without any further purification. The water used in all experiments was deionized.

2.2. Preparation of Oxide Systems

The preparation of the titanium dioxide-zinc oxide systems was realized with two steps. First, TiO₂ was synthesized in the following methodology. To 10% solution of titanium(IV) chloride, a 5 M solution of sodium hydroxide was added (dosing rate of 5 cm³/min) until the pH reached 10. Next, the resulting mixture was transferred to microwave reactor and heated at 200 °C for 10 min at a power of 300 W. The obtained titanium dioxide was filtered, washed three times with deionized water and ethanol, and dried at 105 °C for 12 h. Subsequently, the synthesis of TiO₂-ZnO oxide systems was carried out. In 100 cm³ of a 5% aqueous solution of zinc acetate, 1 g of polyvinylpyrrolidone (PVP)

was added. The received mixture was adjusted to pH 8, with used of 1 M sodium hydroxide solution. After this step, titania obtained in the first step was added as a suspension in water and next resulting mixture was stirred for 30 min. Finally, the obtained mixture was subjected to microwave treatment at 150 °C for 10 min at a power of 300 W. The synthesized materials were filtered and washed three times with deionized water and ethanol and dried at 60 °C for 6 h. Additionally, for comparison purposes, titanium dioxide and zinc oxide samples obtained as reference samples.

2.3. Characterization of Obtained Oxide Systems

The characterization of the physicochemical parameters of the fabricated TiO₂-ZnO oxide systems included the investigation of morphology in particular shape and size of particles (SEM and TEM microscopy) and crystallography (XRD) analysis. Additionally, determination of the parameters of the porous structure using low-temperature N₂ sorption [21–23] has been conducted.

2.4. Tests of Photocatalytic and Photovoltaic Properties

The photocatalytic activity of the obtained TiO₂-ZnO oxide systems was tested in the oxidation reaction system using UV-Vis irradiation. The methodology of photocatalytic tests was presented in our previous work [21]. Additionally, studies related to fabrication of dye sensitized solar cell was carried out. Defining parameters such as preparation of DSSC, dye loading and photovoltaic characteristics were presented in the research article [24].

3. Results and Discussion

3.1. Morphology

In the first stage of the physicochemical analysis of the obtained TiO₂-ZnO systems, scanning and transmission electron microscopy (SEM and TEM) was carried out (Figure 1). The techniques mentioned above were used to determine the morphology (shape and size) of the particles of selected oxide systems ((7)TiO₂-(3)ZnO, (5)TiO₂-(5)ZnO, (3)TiO₂-(7)ZnO) and reference samples.

The presented images for the reference TiO₂ sample show the existence of well-formed nanoparticles of various shapes, e.g. overlong (<50 nm) and also octahedral (<25 nm). However, it should be noted that the obtained nanoparticles tend to form larger aggregates (~ 200 nm), which can be observed in the SEM image presented. Whereas for ZnO, overlong particles (~ 400-500 nm) and nanosheets (<250 nm) were observed. The occurrence of two morphological varieties of ZnO is related to the conditions of synthesis, especially with influence of pH on the shape of the synthesized particles, which was described, among others, by Motshekg et al. [25], as well as Ludi et al. [26].

Based on the SEM and TEM results, it was shown that TiO₂-ZnO oxide systems are characterized by the presence of both TiO₂ nanoparticles and morphological forms corresponding to the ZnO phase. For sample (7)TiO₂-(3)ZnO, the occurrence of single ZnO nanostructures, which were, to some extent, covered with aggregated of TiO₂ nanoparticles, was observed. In the case of oxide systems formed at the molar ratio of TiO₂:ZnO=5:5 and 3:7, a similar morphology was observed. Moreover, based on the interpretation of TEM images, it was indicated that TiO₂ particles are incorporated on the surface of ZnO nanostructures.

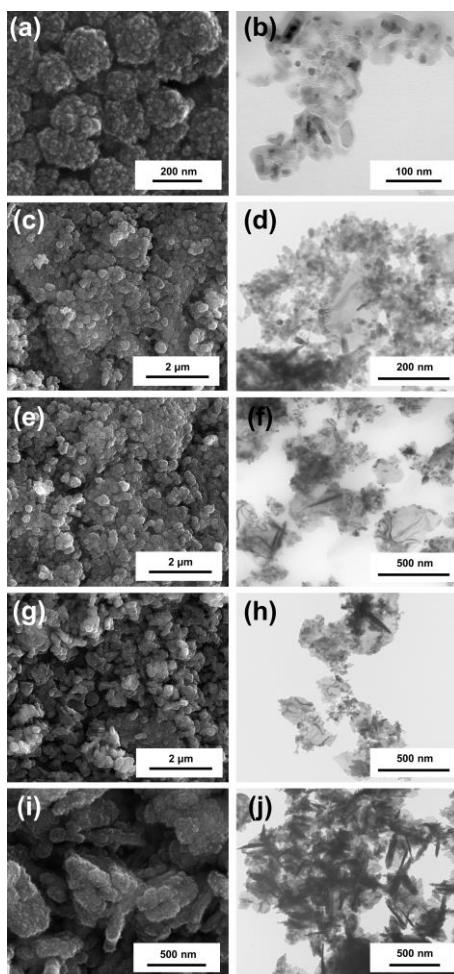


Figure 1. SEM and TEM images for TiO₂ (a,b), (7)TiO₂-(3)ZnO (c,d), (5)TiO₂-(5)ZnO (e,f), (3)TiO₂-(7)ZnO (g,h), ZnO (i,j).

3.2. Crystalline Structure

In order to determine the characteristics of the crystalline structure of the TiO₂-ZnO oxide systems and reference samples, XRD analysis (Figure 2) was performed.

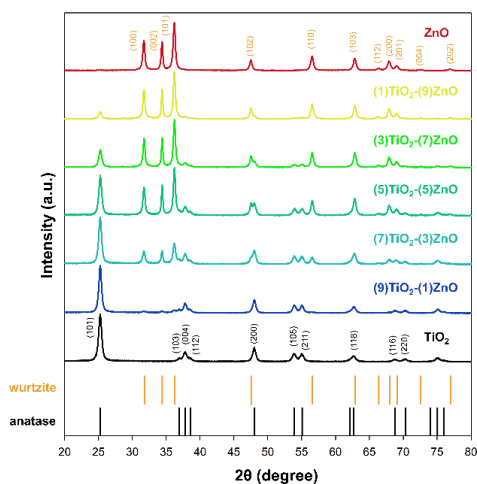


Figure 2. XRD patterns for TiO₂-ZnO oxide systems and reference samples synthesized using the microwave method.

On the XRD pattern for the titanium dioxide sample, the diffraction peaks characteristic of the anatase crystalline structure (card no. 9009086) [13,27] were observed. On the other hand, on the diffraction pattern for the reference ZnO sample, diffraction reflections corresponding to the structure of the wurtzite (card no. 2300112) [28,29] were noted. Based on the crystallography results for two-component materials, it was shown that regardless of the molar ratio of TiO₂:ZnO, diffraction reflections corresponding to both anatase and wurtzite structures were observed. Due to the changes in the intensity of the diffraction peaks corresponding to the structures mentioned above, in the next step, it was decided to determine the phase compositions and the average crystallite size of the analyzed materials (Table 1).

Table 1. Determination of the phase compositions and average crystallite size for TiO₂-ZnO oxide systems and reference samples synthesized using the microwave method.

Sample	Phase Composition (%)		Crystallinity Size (nm)	
	Anatase	Wurtzite	Anatase	Wurtzite
TiO ₂	100(1)	–	14.6 (±0.1)	–
(9)TiO ₂ -(1)ZnO	92(2)	8(1)	16.5 (±0.1)	20.7 (±0.8)
(7)TiO ₂ -(3)ZnO	74(1)	26(1)	15.7 (±0.1)	23.1 (±0.4)
(5)TiO ₂ -(5)ZnO	54(3)	46(2)	15.8 (±0.1)	25.2 (±0.2)
(3)TiO ₂ -(7)ZnO	34(1)	66(2)	15.7 (±0.2)	25.2 (±0.1)
(1)TiO ₂ -(9)ZnO	16(2)	84(1)	15.3 (±0.1)	25.3 (±0.2)
ZnO	–	100(3)	–	25.7 (±0.1)

According to the presented results (Table 1), it was shown that the obtained phase compositions correspond well with the theoretical molar ratios of the components that make up the oxide system. On this basis, it was found that by the proper selection of the TiO₂:ZnO molar ratio, it is possible to obtain oxide systems with a specific phase composition. Besides, it was confirmed that the use of two-stage microwave synthesis allows for obtaining materials with both anatase and wurtzite structures. Furthermore, it was found that for the reference TiO₂ and ZnO samples, the crystallite size is 14.6 nm and 25.7 nm, respectively. What is important, for the oxide systems, similar values of the crystallite size are observed as for the samples mentioned above. Furthermore, the observed slight increase in the size of anatase crystallites for two-component materials (15.3–16.5 nm) is the result of subjecting the crystalline TiO₂ to microwave reprocessing during the formation of oxide systems. For the structure of wurtzite, an increase in the size of crystallites is observed along with an increase in the ZnO content in the synthesized two-component materials (increase in the molar ratio of ZnO). The presented results of diffraction analysis indicate that the application of the two-stage microwave method allowed to obtain TiO₂-ZnO materials with a well-formed structure of both anatase and wurtzite. Moreover, a significant influence of the molar ratio of TiO₂:ZnO on the formation of crystal structures with a specific phase composition was noted.

3.3. Parameters of the Porous Structure

Low-temperature nitrogen sorption was performed to determine the parameters of the porous structure. The obtained N₂ adsorption-desorption isotherms are shown in Figure 3, additionally the determined parameters of the porous structure of the obtained two-component materials are summarized in Table 2.

Based on the obtained nitrogen sorption isotherms, it was shown that the synthesized oxide materials, either the reference samples and the TiO₂-ZnO oxide systems, are characterized by the isotherm type IV with the H3 hysteresis loop [30]. The H3 type hysteresis loop indicates that the analyzed material consists of aggregates of plaque-like particles [30], which create slit pores. Additionally, for both the reference samples and the systems formed at the ratio of TiO₂:ZnO=9:1, 5:5 and 1:9, the same range of hysteresis loop was observed $p/p_0 = 0.8-0.98$. Only for materials (7)TiO₂-(3)ZnO and (3)TiO₂-(7)ZnO, the hysteresis loop shift in the p/p_0 range—0.75–0.98 was noted.

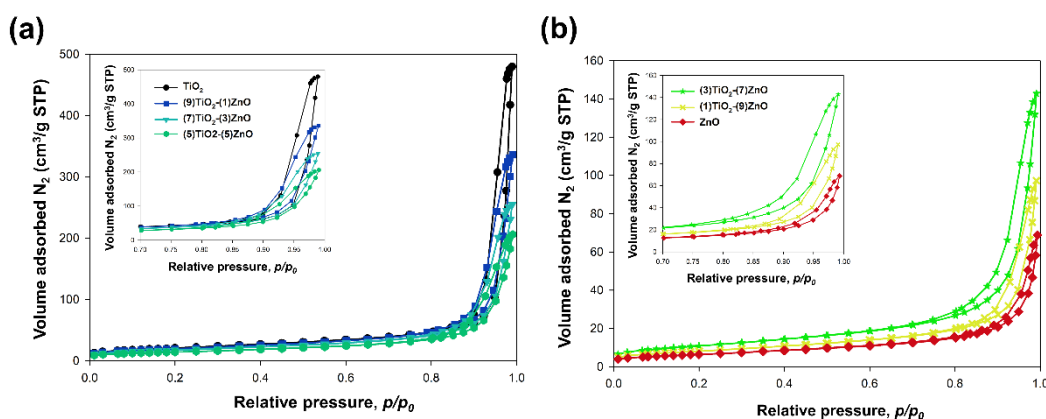


Figure 3. Nitrogen adsorption-desorption isotherms for the following materials: TiO₂, (9)TiO₂-(1)ZnO, (7)TiO₂-(3)ZnO (5)TiO₂-(5)ZnO (a) and (3)TiO₂-(7)ZnO, (1)TiO₂-(9)ZnO and ZnO (b). The hysteresis loops are shown as the inner plot.

Among all synthesized materials, the reference material TiO₂ had the highest surface area (73 m²/g), as well as pore volume (0.75 cm³/g) and pore diameter (37.9 nm). The reference ZnO sample was characterized by the lowest parameters— $A_{BET} = 22$ m²/g; $V_p = 0.11$ cm³/g and $S_p = 17.3$ nm. While the parameters of the porous structure determined for the TiO₂-ZnO oxide systems were between the values mentioned above of the surface area and the volume and average pore diameter.

Table 2. Parameters of the porous structure of TiO₂-ZnO oxide systems and reference samples synthesized via microwave method.

Sample	A_{BET} (m ² /g)	V_p (cm ³ /g)	S_p (nm)
TiO ₂	73	0.75	37.9
(9)TiO ₂ -(1)ZnO	69	0.52	27.3
(7)TiO ₂ -(3)ZnO	62	0.41	21.8
(5)TiO ₂ -(5)ZnO	50	0.32	20.5
(3)TiO ₂ -(7)ZnO	39	0.22	20.1
(1)TiO ₂ -(9)ZnO	29	0.15	18.5
ZnO	22	0.11	17.3

Based on the presented results, it was shown that the molar ratio of the reactants had a significant impact on the parameters of the porous structure, in particular the value of the surface area and the average pore diameter. Additionally, all analyzed materials were characterized by the type IV nitrogen sorption isotherm and the H3 type hysteresis loop. It should be indicated that the relatively low surface area is associated with a well-shaped crystalline structure - comparing the obtained results with the above-presented crystallographic data. Additionally, the observed H3 hysteresis loop, is characteristic for the slit pores, corresponds well with SEM/TEM observations, where the oblong lamellar shape of ZnO forms (nanosheets) was indicated.

3.4. DRS Analysis

Due to the semiconductor properties of the components included in the synthesized two-component materials, the analysis of diffuse reflection spectroscopy was performed. Table 3 presents the results of the DRS analysis performed.

Table 3. The value of the bandgap energy for TiO₂-ZnO oxide systems and reference samples synthesized using the two-stage microwave method.

Sample	E _g (eV)
TiO ₂	3.20
(9)TiO ₂ -(1)ZnO	3.20
(7)TiO ₂ -(3)ZnO	3.15
(5)TiO ₂ -(5)ZnO	3.15
(3)TiO ₂ -(7)ZnO	3.11
(1)TiO ₂ -(9)ZnO	3.10
ZnO	3.10

The interpretation of the graphs of the Kubelka-Munk function as a function of energy, the energy gap was determined. Value of band gap energy equaled 3.2 and 3.1 eV for reference samples TiO₂ and ZnO, respectively. The obtained band gap energy results for titanium dioxide and zinc oxide are consistent with the values presented in the scientific literature [13,28,31]. However, for the synthesized TiO₂-ZnO oxide systems, the E_g values ranging from 3.1 to 3.2 eV were noted, which are identical to the results obtained for the reference samples. The lack of shifts in the value of the bandgap energy results from the fact that the obtained systems consist exclusively of anatase and wurtzite without the presence of mixed structures (including ZnTiO₃).

3.5. Photocatalytic Properties

One of the critical elements of the research was to determine the photocatalytic activity of the synthesized TiO₂-ZnO oxide systems. For this purpose, the process of photocatalytic degradation of the model organic pollutant—phenol (15 mg/dm³) in the range of UV light was carried out, and the obtained results are presented in Figure 4.

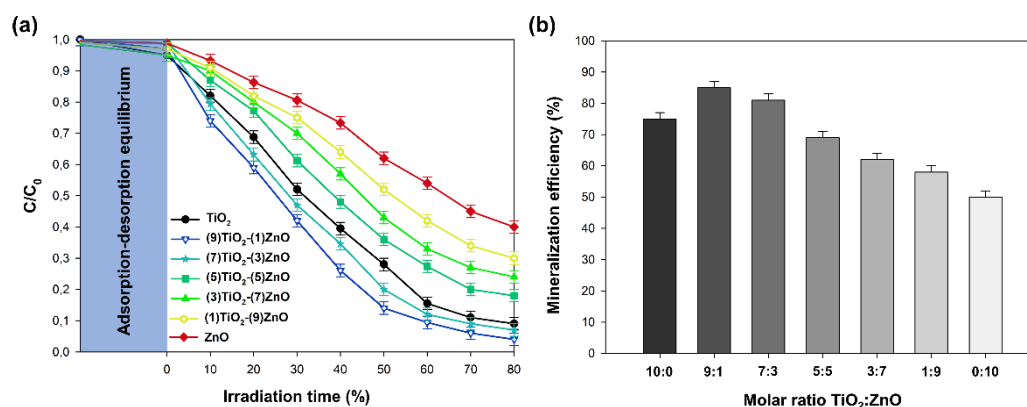


Figure 4. The results of degradation (a) and mineralization (b) of phenol with the use of TiO₂-ZnO oxide systems and reference samples synthesized using the microwave method.

Based on the obtained photodegradation curves, it was shown that the TiO₂ reference sample was characterized by both high degradation efficiency (90%) and mineralization (75%) of phenol after 80 min. Whereas for the reference ZnO sample, the degradation and mineralization efficiency was determined at the level of—60% and 50%, respectively. An improvement in the photocatalytic degradation efficiency of phenol compared to the reference TiO₂ sample was noted for two materials (9)TiO₂-(1)ZnO and (7)TiO₂-(3)ZnO. On the presented photodegradation curves (Figure 4) for the materials mentioned above, the degradation efficiency was 97% and 95%, and the mineralization efficiency was 85% and 81%, respectively. For the material formed at an equimolar ratio of the reactants, the degradation efficiency—80% and the mineralization efficiency—69% were determined. However, for the two-component materials synthesized at the molar ratio of TiO₂:ZnO 3:7 and 1:9, further deterioration of the photocatalytic properties were observed. The analysis of the obtained

results showed that the degradation efficiency of the mentioned materials were 75% and 70%, respectively, while the mineralization efficiency equaled 62% and 58%. Based on the obtained results, it was shown that the prepared TiO₂-ZnO oxide systems are characterized by high efficiency of phenol degradation and mineralization. The highest yield of phenol decomposition was noted for (9)TiO₂-(1)ZnO and (7)TiO₂-(3)ZnO systems, which were shown by the higher efficiency of both degradation and mineralization than the reference samples. The decrease in photocatalytic activity for the remaining materials is probably related to the rapid electron-hole recombination as well as the increase in ZnO content, which may adversely affect the absorption of radiation photons [5,6].

Table 4 shows the comparison of the results from the available scientific literature related to the efficiency of phenol degradation using different photocatalysts.

Table 4. Phenol degradation efficiency using various photoactive materials.

Sample	Concentration of Phenol (mg/dm ³)	Amount of Photocatalyst (mg/100 cm ³)	Degradation Efficiency (%)	Irradiation Time (min)	Ref.
(9)TiO ₂ -(1)ZnO	15	100	97	80	this work
Pt-S-TiO ₂	50	50	100	120	[32]
nano-TiO ₂	40	100	96.0	180	[33]
Co ₃ O ₄ /BiVO ₄	18	300	95	180	[34]
Fe-TiO ₂	100	50	64.5	120	[35]
Ag/ZnO	50	150	100	180	[36]
Pt-ZnO	15	100	90	500	[37]

It should be noted that the photoactivity results of the materials obtained in this study (in particular (9)TiO₂-(1)ZnO) are significantly high in comparison to the effectiveness presented for materials described in other published works (Table 4). Based on the above data, it was indicated that the photocatalysts containing titanium dioxide and zinc oxide in their structure are promising and active photocatalysts in the degradation process of phenol and its derivatives.

3.6. Photovoltaic Properties

In order to characterize the application properties of TiO₂-ZnO oxide systems, the discussed group of materials was used as electrode material in dye-sensitized solar cells.

Tested cells showed variable photovoltaic activity, closely dependent on the electrode material used. By analyzing the registered J-V curves and the photovoltaic parameters obtained (Figure 5 and Table 5), it can be observed that the highest photovoltaic conversion efficiency (η) was demonstrated by the cell utilizing (9)TiO₂-(1)ZnO material. This system's activity is higher than the reference TiO₂ sample and higher than any other material described in the paper. Except for this material, a visible decrease in the photovoltaic process's efficiency can be observed along with the increase in ZnO content in the tested system. The decrease in the efficiency of cells utilizing (7)TiO₂-(3)ZnO and (5)TiO₂-(5)ZnO materials is relatively small.

In contrast, with increasing the ZnO content to at least 70%, a sudden drop in the efficiency of the cells may be observed. By analyzing the remaining parameters of the cells, it should be observed that the main reason for the reduction of the efficiency of the (7)TiO₂-(3)ZnO and (5)TiO₂-(5)ZnO cells is the reduction of the photocurrent density (JSC) while maintaining high values of the open circuit potential (VOC) and fill factor (FF). This situation can be attributed to the effects associated with an increase in the tendency to recombination of excited electrons, along with an increase in the ZnO content in the system, which favours a decrease in the JSC value. However, the still high FF values suggest that the recombination effects in these two materials are not related to the decrease in the ability for the electron transport across the semiconductor material [38,39]. The slight, but evident, increase in the VOC value observed with the increase in ZnO content in the tested materials (except for the systems with the lowest content of TiO₂ and the reference ZnO) could be a consequence of the

differences in the position of the ZnO and TiO₂ conduction band [40,41]. The higher ZnO conduction band level increases the difference between the energy of electrons injected into the semiconductor material, and the reduced form of the redox mediator (present in the electrolyte used) is the main determinant for the VOC value in DSSC [42]. The existence of the energy difference between the TiO₂ and ZnO conduction bands and its influence on the VOC value may also be a reason of the behaviour of the cell based on the (9)TiO₂-(1)ZnO material, the parameters of which are similar to those observed in TiO₂ cells. However, the increased open circuit potential causes an increase in the efficiency of the entire (9)TiO₂-(1)ZnO system.

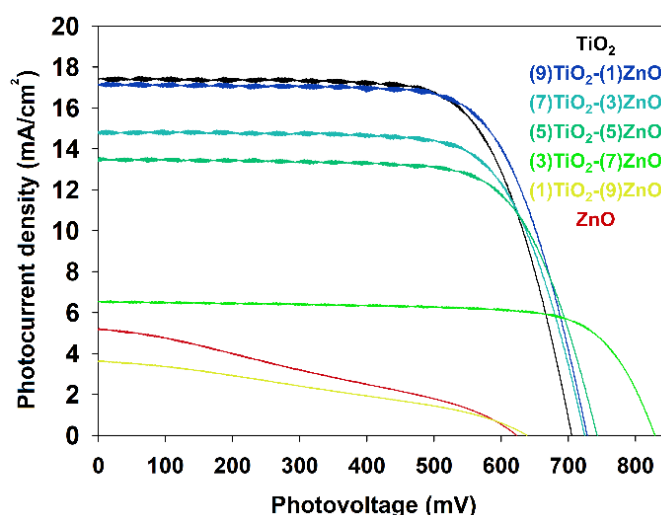


Figure 5. J-V characteristics of the tested solar cells sensitized with dye (DSSC) based on TiO₂-ZnO oxide systems and reference samples synthesized by the two-stage microwave method.

Table 5. Photovoltaic parameters of the investigated cells.

Sample	VOC (mV)	JSC (mA×cm ⁻²)	FF (%)	η (%)
TiO ₂	705	17.5	69.9	8.65
(9)TiO ₂ -(1)ZnO	728	17.3	70.4	8.84
(7)TiO ₂ -(3)ZnO	724	14.9	71.2	7.69
(5)TiO ₂ -(5)ZnO	743	13.6	70.8	7.15
(3)TiO ₂ -(7)ZnO	829	6.57	73.4	4.00
(1)TiO ₂ -(9)ZnO	638	3.65	33.4	0.78
ZnO	623	5.22	31.0	1.01

The electrochemical impedance spectroscopy (EIS) technique has been used to explain the behaviour observed for the tested systems. The EIS results are summarized in Table 6 and presented in Figure 6a,b. The R1 and R2 values, which are the resistance series, mainly dependent on the parameters of the measuring system used, and the resistance of the counter electrode used to build the cells, respectively, do not differ significantly from each other, do not depend on the semiconductor materials used and do not have a more significant impact on differences in their efficiency in the devices discussed [43]. The observed increase of the R2 parameter for the cells (3)TiO₂-(7)ZnO, (1)TiO₂-(9)ZnO, and ZnO is caused by the known effect resulted from the increase of the R3 parameter in these cells [44]. The R3 value, representing the semiconductor/dye/electrolyte interface resistance, is closely related to the semiconductor material used (mainly when one type of dye and electrolyte were applied as in discussed cases). Observation of the R3 value allows explaining the rapid decrease in the activity of (3)TiO₂-(7)ZnO, (1)TiO₂-(9)ZnO and ZnO systems. This apart from the recombination effects discussed earlier, is caused by a sharp increase in the resistance of the semiconductor layer, which significantly impedes transport of the injected electrons inside the cells, translating into their low efficiency. The rapid increase in the R3 resistance also causes a visible

decrease in the FF parameter, reflecting the cells' recombination processes (1)TiO₂-(9)ZnO and ZnO. When comparing the values of the injected electrons lifetime (τ) estimated for individual cells, it can be observed that this parameter is closely related to the VOC values registered for the tested cells. Increasing the lifetime of the injected electrons most often translates into an increase in the photocurrent density, which is in good agreement with the generally observed trend for the first five samples. At the same time, a rapid and too large increase in the τ value for the (1)TiO₂-(9)ZnO and ZnO systems has a negative effect manifested by a significant decrease in the VOC value. This results in the relaxation of the injected electrons because of too strong trapping and preventing their efficient transport inside the semiconductor layer. It can also be caused by a significant increase in the internal resistance of the cells R₃ [45].

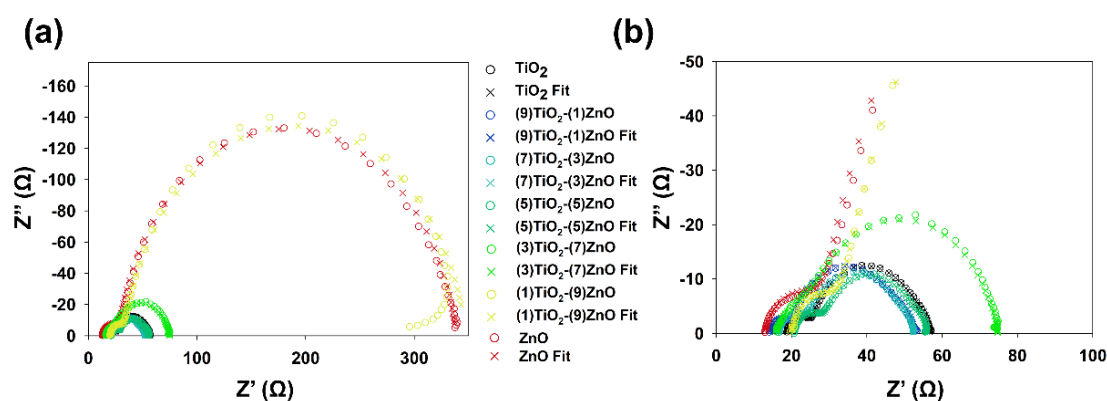


Figure 6. Nyquist graphs of impedance spectra: in the range of 0-300 Ω (a) and 0-100 Ω (b) for DSSC cells based on TiO₂-ZnO oxide systems and reference samples synthesized by the two-stage microwave method.

Table 6. Electrochemical impedance parameters and the amount of adsorbed dye molecules of the investigated cells.

Sample	R ₁ (Ω)	R ₂ (Ω)	R ₃ (Ω)	τ (ms)	N _{dye} (nmol/cm ²)
TiO ₂	18.7	6.4	27.5	5.1	189
(9)TiO ₂ -(1)ZnO	14.1	5.8	26.8	6.4	200
(7)TiO ₂ -(3)ZnO	16.7	7.2	24.4	4.1	189
(5)TiO ₂ -(5)ZnO	20.7	7.6	23.4	3.2	180
(3)TiO ₂ -(7)ZnO	15.7	10.1	46.8	2.5	255
(1)TiO ₂ -(9)ZnO	19.8	12.7	309.7	20.0	245
ZnO	12.9	15.6	310.2	25.1	215

4. Conclusions

First of all, the primary goal of this research was to apply the microwave synthesis to obtain titanium dioxide-zinc oxide systems. Based on the XRD results, the presence of anatase and wurtzite crystalline structures was confirmed. Additionally, it was noted that changing the molar ratio of TiO₂:ZnO affects the crystallographic parameters, such as the phase composition, as well as the average crystallite size, and the morphology and parameters of the porous structure. Contrary to the above-mentioned physicochemical properties, the influence of the TiO₂:ZnO molar ratio on the value of the bandgap energy, which for all systems was ~ 3.1–3.2 eV, was not observed. Analyzing the functional properties of TiO₂-ZnO oxide systems, it was noted that the materials formed using the two-stage microwave method possess the photocatalytic and photovoltaic properties. Based on the photo-oxidation tests was shown that the binary oxide materials (especially the (9)TiO₂-(1)ZnO and (7)TiO₂-(3)ZnO samples) demonstrate high photocatalytic activity in the decomposition of phenol (95% after 80 min irradiation) compared with the reference titania sample. Additionally, the obtained two-component systems were tested as electrode material in dye-sensitized solar cells with

satisfactory results. The best photovoltaic parameters have been found in the case of the (9)TiO₂-(1)ZnO material, which was characterized by an efficiency of 8.84%.

Author Contributions: A.K., synthesis of the materials, research concept, characterization of materials; Z.B. and A.Z.-J., determination of photocatalytic activity and interpretation of results; A.B. and M.Z., determination of photovoltaic properties and interpretation of results; K.S.-C., BET analysis; K.S.-C. and T.J., critical revision and supervision of all aspects of the research. All authors have read and agreed to the published version of the manuscript.

Funding: This research was funded by the Ministry of Science and Higher Education Poland as a subsidy to Poznan University of Technology (grant no. 0912/SBAD/2006).

Conflicts of Interest: The authors declare no conflict of interest.

References

1. Peters, R.L. Effects of global warming on forests. *For. Ecol. Manag.* **1990**, *35*, 13–33.
2. Lehtonen, H. Potential effects of global warming on northern European freshwater fish and fisheries. *Fish. Manag. Ecol.* **1996**, *3*, 59–71.
3. Randazzo, B.; Chemello, G.; Tortarolo, I.; Chiarello, G.L.; Zalas, M.; Santini, A.; Liberatore, M.; Liberatore, M.; Selli, E.; Olivotto, I. A novel photocatalytic purification system for fish culture. *Zebrafish* **2017**, *14*, 1448.
4. Deng, Y.; Tang, L.; Zeng, G.; Wang, J.; Zhou, Y.; Wang, J.; Tang, J.; Wang, L.; Feng, C. Facile fabrication of mediator-free Z-scheme photocatalyst of phosphorous-doped ultrathin graphitic carbon nitride nanosheets and bismuth vanadate composites with enhanced tetracycline degradation under visible light. *J. Colloid Interface Sci.* **2018**, *509*, 219–234.
5. Ohtani, B. Photocatalysis A to Z—What we know and what we do not know in a scientific sense. *J. Photochem. Photobiol. C Photochem. Rev.* **2010**, *11*, 157–178.
6. Ohtani, B. Titania photocatalysis beyond recombination: A critical review. *Catalysts* **2013**, *3*, 942–953.
7. Kowalska, E.; Abe, R.; Ohtani, B. Visible light-induced photocatalytic reaction of gold-modified titanium(IV) oxide particles: Action spectrum analysis. *Chem. Commun.* **2009**, 241–243.
8. Zielińska-Jurek, A.; Kowalska, E.; Sobczak, J.W.; Lisowski, W.; Ohtani, B.; Zaleska, A. Preparation and characterisation of monometallic (Au) and bimetallic (Ag/Au) modified-titania photocatalysts activated by visible light. *Appl. Catal. B Environ.* **2011**, *101*, 504–514.
9. Kowalska, E.; Janczarek, M.; Rosa, L.; Juodkazis, S.; Ohtani, B. Mono- and bi-metallic plasmonic photocatalysts for degradation of organic compounds under UV and visible light irradiation. *Catal. Today* **2014**, *230*, 131–137.
10. Su, Y.; Nathan, A.; Ma, H.; Wang, H. Precise control of Cu₂O nanostructures and LED-assisted photocatalysis. *RSC Adv.* **2016**, *6*, 78181–78186.
11. Casado, C.; Timmers, R.; Sergejevs, A.; Clarke, C.T.; Allsopp, D.W.E.; Bowen, C.R.; van Grieken, R.; Marugán, J. Design and validation of a LED-based high intensity photocatalytic reactor for quantifying activity measurements. *Chem. Eng. J.* **2017**, *327*, 1043–1055.
12. Baruah, S.; Dutta, J. Hydrothermal growth of ZnO nanostructures. *Sci. Technol. Adv. Mater.* **2009**, *10*, 013001.
13. Kubiak, A.; Siwińska-Ciesielczyk, K.; Jesionowski, T. Titania-based hybrid materials with ZnO, ZrO₂ and MoS₂: A review. *Materials* **2018**, *11*, 2295.
14. Jankowska, K.; Zdarta, J.; Grzywaczyk, A.; Kijeńska-Gawrońska, E.; Biadasz, A.; Jesionowski, T. Electrospun poly(methyl methacrylate)/polyaniline fibres as a support for laccase immobilisation and use in dye decolourisation. *Environ. Res.* **2020**, *184*, 109332.
15. Arami, H.; Mazloumi, M.; Khalifehzadeh, R.; Sadrnezhad, S.K. Sonochemical preparation of TiO₂ nanoparticles. *Mater. Lett.* **2007**, *61*, 4559–4561.
16. Ramimoghadam, D.; Hussein, M.Z.B.; Taufiq-Yap, Y.H. Synthesis and characterisation of ZnO nanostructures using palm olein as biotemplate. *Chem. Cent. J.* **2013**, *7*, 1–10.
17. Prielcel, P.; Lopez-Sanchez, J.A. Advantages and limitations of microwave reactors: From chemical synthesis to the catalytic valorisation of biobased chemicals. *ACS Sustain. Chem. Eng.* **2019**, *7*, 3–21.
18. Kappe, C.O.; Dallinger, D. The impact of microwave synthesis on drug discovery. *Nat. Rev. Drug Discov.* **2006**, *5*, 51–63.

19. Gupta, D.; Jamwal, D.; Rana, D.; Katoch, A. Microwave synthesised nanocomposites for enhancing oral bioavailability of drugs. In *Applications of Nanocomposite Materials in Drug Delivery*; Asiri, I.A., Ali, M., Eds.; Elsevier Inc.: Amsterdam, Nederland, 2018; pp. 619–632.
20. Roberts, B.A.; Strauss, C.R. Toward Rapid, "Green", Predictable Microwave-Assisted Synthesis. *ChemInform* **2005**, *36*, 653–661.
21. Kubiak, A.; Bielan, Z.; Bartkowiak, A.; Gabała, E.; Piasecki, A.; Zalas, M.; Zielińska-Jurek, A.; Janczarek, M.; Siwińska-Ciesielczyk, K.; Jesionowski, T. Synthesis of titanium dioxide via surfactant-assisted microwave method for photocatalytic and dye-sensitized solar cells applications. *Catalysts* **2020**, *10*, 586–610.
22. Kubiak, A.; Siwińska-Ciesielczyk, K.; Goscińska, J.; Dobrowolska, A.; Gabała, E.; Czaczyk, K.; Jesionowski, T. Hydrothermal-assisted synthesis of highly crystalline titania–copper oxide binary systems with enhanced antibacterial properties. *Mater. Sci. Eng. C* **2019**, *104*, 109839.
23. Kubiak, A.; Wojciechowska, W.; Kurc, B.; Pięłowska, M.; Synoradzki, K.; Gabała, E.; Moszyński, D.; Szybowski, M.; Siwińska-Ciesielczyk, K.; Jesionowski, T. Highly crystalline TiO₂–MoO₃ composite materials synthesized via a template-assisted microwave method for electrochemical application. *Crystals* **2020**, *10*, 1–25.
24. Zalas, M.; Jelak, K. Optimization of platinum precursor concentration for new, fast and simple fabrication method of counter electrode for DSSC application. *Optik* **2020**, *206*, 164314.
25. Motshekga, S.C.; Ray, S.S.; Onyango, M.S.; Momba, M.N.B. Microwave-assisted synthesis, characterisation and antibacterial activity of Ag/ZnO nanoparticles supported bentonite clay. *J. Hazard. Mater.* **2013**, *262*, 439–446.
26. Ludi, B.; Niederberger, M. Zinc oxide nanoparticles: Chemical mechanisms and classical and non-classical crystallisation. *Dalt. Trans.* **2013**, *42*, 12554–12568.
27. Aguir, K.; Bernardini, S.; Lawson, B.; Fiorido, T. Trends in metal oxide thin films: Synthesis and applications of tin oxide. In *Tin Oxide Materials Synthesis, Properties, and Applications*; Orlandi, M.O., Eds.; Elsevier Inc.: Amsterdam, Nederland, 2020; pp. 219–246.
28. Kolodziejczak-Radzimska, A.; Jesionowski, T. Zinc oxide—from synthesis to application: A review. *Materials* **2014**, *7*, 2833–2881.
29. Wojnarowicz, J.; Chudoba, T.; Lojkowski, W. A review of microwave synthesis of zinc oxide nanomaterials: Reactants, process parameters and morphologies. *Nanomaterials* **2020**, *10*, 1086.
30. Sing, K.S.W.; Everett, D.H.; Haul, R.A.W.; Moscou, L.; Pierotti, R.S.; Rouquerol, J.; Siemienińska, T. Reporting physisorption data for gas/solid systems with special reference to the determination of surface area and porosity. *Pure Appl. Chem.* **1985**, *57*, 603–619.
31. McCullagh, C.; Robertson, J.M.C.; Bahnemann, D.W.; Robertson, P.K.J. The application of TiO₂ photocatalysis for disinfection of water contaminated with pathogenic micro-organisms: A review. *Res. Chem. Intermed.* **2007**, *33*, 359–375.
32. Murcia, J.J.; Hidalgo, M.C.; Navío, J.A.; Araña, J.; Doña-Rodríguez, J.M. Study of the phenol photocatalytic degradation over TiO₂ modified by sulfation, fluorination, and platinum nanoparticles photodeposition. *Appl. Catal. B Environ.* **2015**, *179*, 305–312.
33. Ray, S.; Lalman, J.A.; Biswas, N. Using the Box-Benken technique to statistically model phenol photocatalytic degradation by titanium dioxide nanoparticles. *Chem. Eng. J.* **2009**, *150*, 15–24.
34. Long, M.; Cai, W.; Cai, J.; Zhou, B.; Chai, X.; Wu, Y. Efficient photocatalytic degradation of phenol over Co₃O₄/BiVO₄ composite under visible light irradiation. *J. Phys. Chem. B* **2006**, *110*, 20211–20216.
35. Borji, S.H.; Nasser, S.; Mahvi, A.H.; Nabizadeh, R.; Javadi, A.R. Photocatalytic degradation of phenol in aqueous solutions by Fe(III)-doped TiO₂/UV process. *J. Environ. Health. Sci. Eng.* **2014**, *12*, 369–380.
36. Vaiano, V.; Matarangolo, M.; Murcia, J.J.; Rojas, H.; Navío, J.A.; Hidalgo, M.C. Enhanced photocatalytic removal of phenol from aqueous solutions using ZnO modified with Ag. *Appl. Catal. B Environ.* **2018**, *225*, 197–206.
37. Morales-Flores, N.; Pal, U.; Sánchez Mora, E. Photocatalytic behavior of ZnO and Pt-incorporated ZnO nanoparticles in phenol degradation. *Appl. Catal. A Gen.* **2011**, *394*, 269–275.
38. Biswas, S.; Hossain, M.F.; Takahashi, T. Fabrication of Grätzel solar cell with TiO₂/CdS bilayered photoelectrode. *Thin Solid Films* **2008**, *517*, 1284–1288.
39. Pradhan, B.; Batabyal, S.K.; Pal, A.J. Vertically aligned ZnO nanowire arrays in Rose Bengal-based dye-sensitized solar cells. *Sol. Energy Mater. Sol. Cells* **2007**, *91*, 769–773.

40. Park, S.K.; Kim, C.; Kim, J.H.; Bae, J.Y.; Han, Y.S. Effects of Mg salt-modified TiO₂ on the photovoltaic performance of dye-sensitised solar cells. *Curr. Appl. Phys.* **2011**, *11*, 131–135.
41. Sharma, G.D.; Suresh, P.; Roy, M.S.; Mikroyannidis, J.A. Effect of surface modification of TiO₂ on the photovoltaic performance of the quasi solid state dye sensitised solar cells using a benzothiadiazole-based dye. *J. Power Sources* **2010**, *195*, 3011–3016.
42. Hagfeldt, A.; Boschloo, G.; Sun, L.; Kloo, L.; Pettersson, H. Dye-Sensitized Solar Cells. *Chem. Rev.* **2010**, *110*, 6595–6663.
43. Bartkowiak, A.; Orwat, B.; Zalas, M.; Ledwon, P.; Kownacki, I.; Tejchman, W. 2-Thiohydantoin moiety as a novel acceptor/anchoring group of photosensitisers for dye-sensitised solar cells. *Materials* **2020**, *13*, 2065.
44. Sakthivel, T.; Kumar, K.A.; Senthilselvan, J.; Jagannathan, K. Effect of Ni dopant in TiO₂ matrix on its interfacial charge transportation and efficiency of DSSCs. *J. Mater. Sci. Mater. Electron.* **2018**, *29*, 2228–2235.
45. Mozer, A.J.; Wagner, P.; Officer, D.L.; Wallace, G.G.; Campbell, W.M.; Miyashita, M.; Sunahara, K.; Mori, S. The origin of open circuit voltage of porphyrin-sensitised TiO₂ solar cells. *Chem. Commun.* **2008**, *39*, 4741–4743.

Publisher's Note: MDPI stays neutral with regard to jurisdictional claims in published maps and institutional affiliations.



© 2020 by the authors. Submitted for possible open access publication under the terms and conditions of the Creative Commons Attribution (CC BY) license (<http://creativecommons.org/licenses/by/4.0/>).